

# Molecular dynamics simulations of the interactions between triose phosphate isomerase and sulfonamides

Neville Y. Forlemu and Joseph Sloop

School of Science and Technology (Chemistry), Georgia Gwinnett College, Lawrenceville, GA, USA

## ABSTRACT

Malaria is a disease with debilitating health and negative economic impacts in regions at high risk of infection. Parasitic resistance and side effects of current antimalarial drugs are major setbacks to the successful campaigns that have reduced malaria incidence by 40% in the last decade. The parasite's dependence on glycolysis for energy requirements makes pathway enzymes suitable targets for drug development. Specifically, triose phosphate isomerase (TPI) from *Plasmodium falciparum* (pTPI) and human (hTPI) cells show striking structural features that can be used in development of new antimalarial agents. In this study MD simulations were used to characterize binding sites on hTPI and pTPI interactions with sulfonamides. The molecular mechanics Poisson–Boltzmann surface area (MM–PBSA) method was used to estimate the interaction energies of four sulfonamide-TPI docked complexes. A unique combination of key residues at the dimer interface of pTPI is responsible for the observed selective affinity to pTPI compared to hTPI. The representative sulfonamide; 4-amino-N-(3,5-dimethylphenyl)-3-fluorbenzenesulfonamide (sulfaE) shows a strong affinity with pTPI (dimer interface,  $-42.91\text{ kJ/mol}$  and active site region,  $-71.62\text{ kJ/mol}$ ), hTPI (dimer interface,  $-41.32\text{ kJ/mol}$  and active site region,  $-84.40\text{ kJ/mol}$ ). Strong and favorable Van der Waals interactions and increases in non-polar solvation energies explain the difference in affinity between pTPI with sulfaE compared to hTPI at the dimer interface. This is an indication that the dimer interface of TPI glycolytic enzyme is vital for development of sulfonamide based antimalarial drugs.

Submitted 27 September 2019  
Accepted 18 August 2020  
Published 3 September 2020

Corresponding author

Neville Y. Forlemu,  
nforlemu@ggc.edu

Academic editor  
Ho Leung Ng

Additional Information and  
Declarations can be found on  
page 19

DOI 10.7717/peerj-pchem.13

© Copyright  
2020 Forlemu and Sloop

Distributed under  
Creative Commons CC-BY 4.0

OPEN ACCESS

**Subjects** Theoretical and Computational Chemistry, Biophysical Chemistry, Physical Chemistry (other), Thermodynamics and Statistical Mechanics, Molecular and Collisional Dynamics

**Keywords** Malaria, Glycolytic enzymes, Triosephosphate isomerase, Binding energy, Sulfonamides, *Plasmodium falciparum*, MM–PBSA, MD simulations

## INTRODUCTION

Parasitic organisms, such as *Plasmodium* with a fully compartmentalized glycolytic pathway, are responsible for the world scourge of malaria prevalent in tropical and sub-tropical regions of the world (*Kehr et al., 2010*). Malaria, if untreated, can lead to very debilitating conditions such as coma, brain damage, loss of muscle function and death (*Ringwald et al., 2002*). Global mapping data estimates that about 3.2 billion people are at risk of contracting malaria every year (*Guerra, Snow & Hay, 2006*).

Aniline- and sulfonamide-based drugs like sulfadoxine have been shown to interfere with the production of cellular components (amino acids and nucleotides), important for cell growth in parasitic organisms (*Plasmodium* and bacteria) (Hyde, 2007). Folate pathway enzymes like dihydropteroate synthase and dihydrofolate reductase are major targets for malaria treatment using combination therapy of sulfadoxine-pyrimethamine (SP) (Matondo et al., 2014; Mulenga et al., 2006). The continued application of the SP combination in place of the more effective artemisinin-based combination therapy is due to minimal side effects. Despite the limited efficacy of SP because of parasitic resistance resulting from genetic mutations, the World Health Organization continues to recommend their use in heavily affected regions mainly for safety concerns (Djaman et al., 2004; Heinberg & Kirkman, 2015). One of the goals of this study is to explore whether the sulfonamides we have designed can selectively interact with target receptors critical to the *Plasmodium* parasite.

The *Plasmodium* parasite's sole dependence on glycolysis for energy needs makes the pathway enzymes potential targets for development of antimalarial chemotherapies (Kim & Dang, 2005; Velanker et al., 1997; Verlinde et al., 2001). The decrease in efficiency of current antimalarial agents in many affected regions of the world due to toxic side effects, parasitic resistance caused by mutation has increased the cost and complexity of treating malaria (Bray et al., 2003; Briolant et al., 2010; Petersen, Eastman & Lanzer, 2011). The limited number of new and effective antimalarial drugs, coupled with parasitic resistance to almost every available therapeutic combination continues to spur the search for novel, cheaper and better analogues (Plowe et al., 2007; Triglia et al., 1997). Triosephosphate isomerase (TPI) is a key dimeric enzyme that speeds up the final investment phase of glycolysis, especially necessary for energy production in *Plasmodium* parasite the causative agent of malaria. TPI is an efficient enzyme that catalyzes the reversible interconversion between two triose phosphates; dihydroxyacetone phosphate (DHAP) and glyceraldehyde-3-phosphate (G3P) (Richard, 1985). The three-dimensional structures of human TPI (hTPI) with PDB accession code 4POC, (Roland et al., 2015) and *Plasmodium* TPI (pTPI) with PDB accession code-2VFI (Gayathri et al., 2009) share similar structural folds (0.825 Å root mean square deviation in atomic positions), despite the 58% difference in sequence identity (Fig. 1). TPI enzymes do however, have key amino acid residues located in key binding motifs with different side chain polarities (Fig. 1B). The two motifs of significant interest so far in the literature include; the dimer interface and active site regions. For example, position 96 that is proximal to TPI active site residues (K12, H95 and E165) in many TPI sequences is usually occupied by serine. This is replaced by Phenylalanine (Phe) in pTPI sequence (Parthasarathy et al., 2002). In TPI the dimer interface comprises of residues (Y48, D49, V46, S45) that face each other and extend the electrostatic field of this binding motif (Figs. 2A and 2B). We also observe some subtle substitutions that affect the size and polarity of interface residues. The red and blue regions correspond to extreme values (low and high) electrostatic potential energy representative of surfaces occupied by polar acidic and basic residues. The green to white regions indicate intermediary electrostatic potential, energy representative surfaces occupied by nonpolar residues.

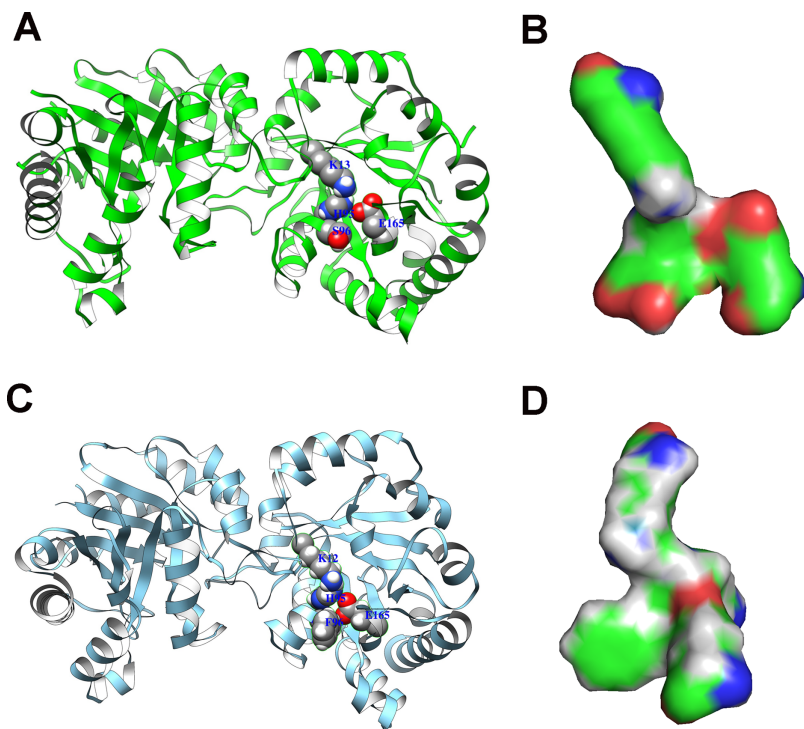


**Figure 1** Active site residues TPI. (A) hTPI (green) structure with active site residues and (B) Electrostatic potential surface of hTPI active site. (C) pTPI (cyan) structure with active site residues and (D). Electrostatic potential surface of pTPI active site. Active site surface polarity variation in part due to substitution of S96 in hTPI-to F96 in pTPI.

Full-size DOI: 10.7717/peerj-pchem.13/fig-1

For example, A46, I48 in hTPI are replaced by V46, Y48 in pTPI. As a result, the dimer interface in pTPI seems more polar and less tight compared to hTPI (Fig. 2).

In our previous work, molecular docking calculations of the interaction between glycolytic enzymes with sulfanilamide, antimalarial drugs (primaquine, pyrimethamine, chloroquine) and eight fluorinated sulfonamides (*Dizala-Mukinay et al., 2017; Forlemu, Watkins & Sloop, 2017*) classified the compounds in low and high affinity groups with potential of selectivity. The sulfonamides we tested are derivatives of sulfadoxine that is used in combination with pyrimethamine to treat malaria in children and pregnant women (*Menard & Dondorp, 2017*). Our docking calculations identified three sulfonamide ligands with strong binding affinity in micromolar range, and enhance interactions with pTPI over to hTPI (Table 1). The affinity of the three novel sulfonamides docked with TPI was also significantly stronger than a number of antimalarial drugs (quinine, pyrimethamine and primaquine) (*Forlemu, Watkins & Sloop, 2017*).

Despite the initial success of the docking studies to identify TPI as a target receptor, with potential of enhanced selectivity between hTPI and pTPI, the inhibition mechanism, dynamic motions of enzymes upon binding and contribution of residues is not well understood. In the current study, we have performed molecular dynamics (MD) simulations on four ternary complexes with the representative sulfonamide docked in the identified binding modes. Our goal is to gain insights on the binding process and explanation of the impact of residue substitutions like S96 in hTPI–F96 in pTPI and dimer

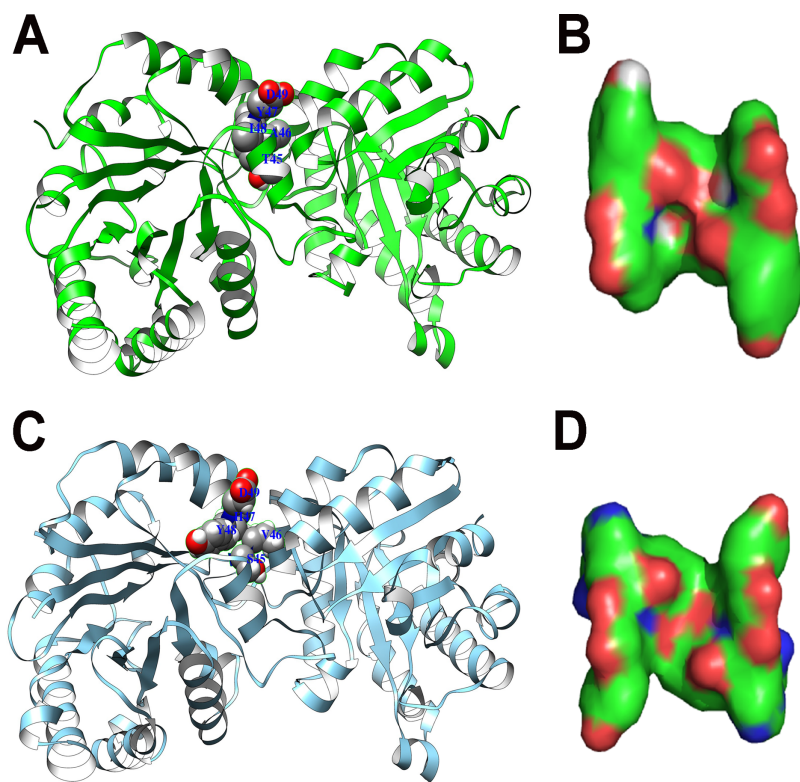


**Figure 2** Dimer interface residues TPI. (A) The dimer interface of human TPI enzyme and (B) electrostatic potential surface of key residues (A45-I48). (C) The dimer interface of *Plasmodium* TPI enzyme and (D) electrostatic potential surface of some key residues (V45-Y48).

Full-size DOI: 10.7717/peerj-pchem.13/fig-2

**Table 1** Molecular docking binding energies between sulfonamides and hTPI/pTPI.

Ligand	SulfaE	SulfaC	SulfaH
Name	4-amino-N-(3,5-dimethylphenyl)-3-fluorbenzenesulfonamide	4-amino-N-(2-fluoro-3,5-dimethylphenyl)benzenesulfonamide	4-amino-N-(2,6-difluorophenyl)-2,6-dimethoxybenzene sulfonamide
hTPI	-6.84 ( $\pm$ 0.23) kcal/mol	-7.10 ( $\pm$ 0.46) kcal/mol	-6.15 ( $\pm$ 0.85) kcal/mol
pTPI	-9.50 ( $\pm$ 0.43) kcal/mol	-9.70 ( $\pm$ 0.76) kcal/mol	-8.45 ( $\pm$ 0.53) kcal/mol

interface residues substitutions. We hypothesize that the size and changes in polarity of the amino acid substitution A46, I48 in hTPI-V46, Y48 in pTPI, enhances affinity for sulfonamides. Chemical structures of the sulfonamide ligands bound to the TPI receptor in the docking study are shown in Fig. 3.

The binding energy ( $\Delta G$ ), residue contribution to energy between a representative sulfonamide ligand 4-amino-N-(3,5-dimethylphenyl)-3-fluorbenzenesulfonamide (sulfaE) with hTPI and pTPI was calculated by the molecular mechanics/Poisson–Boltzmann and surface area solvation method. We expect to obtain answers to two key questions: (1) Is there some selective enhancement for the binding of sulfonamide to hTPI as opposed

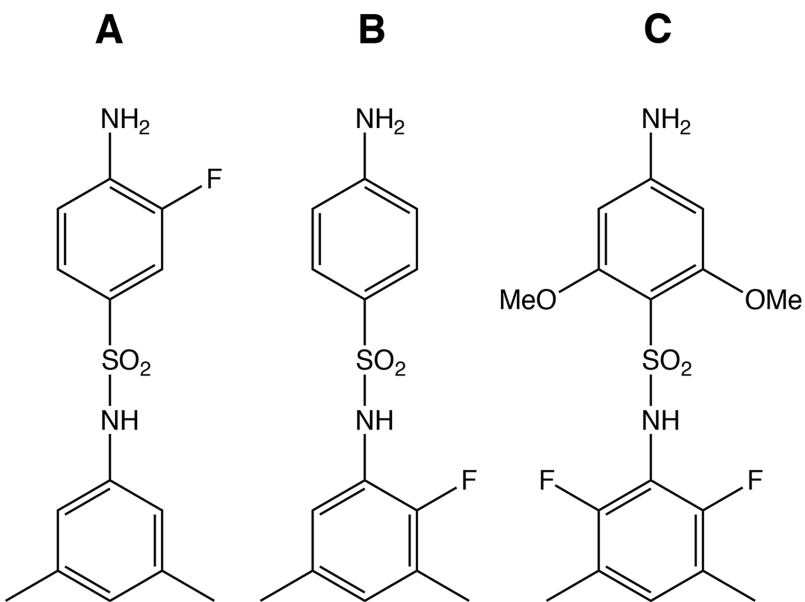


**Figure 3 Sulfonamides.** Chemical structures of docked ligands with highest affinity and selectivity; (A) SulfaE; (B) sulfaC and (C) SulfaH. The full names and affinities on [Table 1](#).

Full-size DOI: [10.7717/peerj-pchem.13/fig-3](https://doi.org/10.7717/peerj-pchem.13/fig-3)

to pTPI? (2) What structural motifs and residues are critical for the binding, and are the key TPI residue substitutions critical for binding sulfonamides? Docked complexes obtained from using AutoDock 4.2 served as initial configurations for MD simulations (Gromacs software package) to screen impactful interactions and dynamically refined the complexes formed ([Van Der Spoel et al., 2005](#)).

## MOLECULAR SYSTEMS AND COMPUTATIONAL METHODS

### Docked complexes and ligands

The interactions between eight novel sulfonamides with hTPI and pTPI were characterized using blind docking ([Forlemu, Watkins & Sloop, 2017](#)). The docking scores for the best performing sulfonamides 4-amino-N-(3,5-dimethylphenyl)-3-fluorobenzenesulfonamide (sulfaE), 4-amino-N-(2-fluoro-3,5-dimethylphenyl)-benzenesulfonamide (sulfaC) and 4-amino-N-(2,6-difluorophenyl)-2,6-dimethoxybenzenesulfonamide (sulfaH) are shown in [Table 1](#). The three-dimensional structures of the ligands tested were built using GuassView, and then geometry optimized with Gaussian 09 using a B3LYP/6-311g basis set ([Dennington, Keith & Millam, 2009](#); [Frisch et al., 2016](#)). The derivatives have the same basic structure, but differ in the substitution pattern of polar fluorine, methoxy and alkyl functional groups ([Table 1](#); [Fig. 3](#)). The binding energies from docking calculations for all three high affinity sulfonamides are not significantly different as a result only sulfaE configuration is used as a representative sulfonamide for the MD simulations. SulfaE docked complexes were used as initial MD input structures based on enhanced selectivity in terms of affinity (binding energies and dissociation constant) with pTPI compared to hTPI. ([Forlemu, Watkins & Sloop, 2017](#)). The molecular topologies and parameters for sulfaE were obtained from the fast force field generating tool called SwissParam

(Zoete *et al.*, 2011), based on the Merck molecular force field. The molecular mechanics Poisson–Boltzmann surface area (MM–PBSA) method was used to estimate the interaction energies of four sulfonamide-TPI docked complexes (Homeyer & Gohlke, 2012).

## MD simulations

Molecular dynamics simulations were carried out on four sulfaE/TPI docked complexes. The first two complexes involved sulfaE docked in the dimer or active site region of pTPI and the other two involving sulfaE docked in the dimer or active site region of hTPI. Each docked complex was relaxed using two stages of 1,000 steps of steepest decent energy minimization, followed by 50,000 steps of conjugate gradient energy minimization. Subsequently a 4-ns long MD simulation was used to equilibrate each system at 300 K using an NVT ensemble, with GROMACS MD code and a V-rescale thermostat to keep the temperature fixed (Bussi, Donadio & Parrinello, 2007). This was followed by a 10 ns NPT ensemble simulation to equilibrate the pressure at 1 bar and 300 K. A final production MD was run for 500 ns, with atomic coordinates saved after every 100 ps. All the simulations were performed using the TIP3P water model and the protein described using the CHARMM27 force field (Foloppe, MacKerell & Alexander, 2000; Jorgensen *et al.*, 1983). The simulations were performed in an orthorhombic box with periodic boundary conditions and dimensions at least 8 Å from the solute (protein ligand complex). The complex was soaked in water molecules for a total system size of 93 Å × 87 Å × 76 Å. The total system charge was kept neutral by using an appropriate combination of chloride and sodium ions. The PME method was used to estimate the long-range electrostatic interactions, with short range nonbonding interactions estimated using a 14 Å cutoff. The time step for each simulation was set 2 fs and the hydrogens restrained using the SHAKE algorithm (Berendsen *et al.*, 1984; Van Gunsteren & Berendsen, 1977).

## Binding free energy calculation

The MM/PBSA (molecular mechanics (MM) with Poisson–Boltzmann (PB) and surface area solvation) method was used estimate the binding free energy between sulfaE and different binding pockets on pTPI and hTPI (Kollman *et al.*, 2000). The single-trajectory MM/PBSA method was used to post-process the binding energy ( $\Delta G_{\text{bind}}$ ) of four sulfaE (L)/TPI(P) complexes to determine impact of binding pocket and residues substitutions (Scheme 1).



The binding free energy was computed as

$$\Delta G_{\text{bind}} = G_{PL} - G_P - G_L \quad (1)$$

Where  $G$  is computed from molecular mechanics (MM) force field expressions

$$G = E_{\text{bond}} + E_{el} + E_{vdw} + G_{pol} + G_{np} - TS \quad (2)$$

Here  $E_{\text{bond}}$  represents standard molecular mechanics force field terms describe stretching, bending, and torsional bonded interactions (Eq. (3))

$$E_{\text{bond}} = \sum_{\text{bond}} k_B(b - b_0)^2 + \sum_{\text{angle}} k_\theta(\theta - \theta_0)^2 + \sum_{\text{dih}} k_\phi[(1 + \cos(n\phi - \delta))] \quad (3)$$

Where  $k_b$  is a bond stretching constant,  $b$  is the actual length of the bond, and  $b_0$  is the equilibrium bond length,  $k_\theta$  is the angle bending constant,  $\theta$  is the actual angle and  $\theta_0$  the equilibrium or unstrained angle. The phase angle shifts for the torsional angle  $\phi$  is represented by  $\delta$ . The constant  $k_\phi$  controls the amplitude of the bond twist (rotation curves),  $n$  is an integer (2, 3, 4 or 6) that describes the periodicity of the bond twist.

$$E_{el} = \sum_i \sum_{j > i} \frac{q_i q_j}{4\pi\epsilon_0 r_{ij}} \quad (4)$$

$$E_{vdW} = \sum_i \sum_{j > i} 4\epsilon_{ij} \left[ \left( \frac{\sigma_{ij}}{r_{ij}} \right)^{12} - \left( \frac{\sigma_{ij}}{r_{ij}} \right)^6 \right] \quad (5)$$

The nonbonded interactions include the electrostatic interactions approximated by the coulomb potential and van der Waals interactions approximated with the 6–12 Lennard–Jones type potential (Eqs. (4) and (5)). The constants  $\epsilon_{ij}$  are characteristic of the atoms involved,  $\sigma_{ij}$  represents the attractive and repulsive parameters for atoms  $i$  and  $j$  respectively, and  $r_{ij}$  the distance between the centers of the two atoms. The electrostatic interaction is defined by assigning partial charges ( $q_i$  and  $q_j$ ) to each Van der Waals atom. The effective dielectric constant is represented by  $\epsilon_0$ . The solvation energy is captured by an electrostatic polar contribution ( $G_{\text{pol}}$ ) and a non-polar contribution ( $G_{\text{np}}$ ) term. The  $G_{\text{pol}}$  term is obtained from the solution to the Poisson–Boltzmann equation as describe below (Eq. (6)) within the implicit solvent model and describe the free energy solvation contribution

$$\nabla[\epsilon(r)\nabla\phi(r)] - \epsilon(r)\kappa^2 \sinh(\phi(r)) + 4\pi\rho(r) = 0 \quad (6)$$

$$\text{where } \kappa^2 = \frac{8\pi e^2 I}{\epsilon_v k_B T}$$

where  $I$  represent Ionic strength (0.15 M),  $\epsilon_v$  the dielectric constant (1 and 80 for receptor and water respectively) and thus implicitly accounting for solvent properties.  $G_{\text{np}}$  describes the non-polar contributions to the solvation energy and can be determined from the solvent accessible surface area approximation (SASA) (Homeyer & Gohlke, 2012).

The MM–PBSA is an intermediate free energy calculation method that has been shown to estimate ligand binding affinities with correlation coefficients comparable to experiments and also discriminate between ligand protein complexes better than the widely used docking methods. In this study, the average binding energies and other quantities of interest are computed using structures from 500 snapshots selected from the last 400 ns of the 1 ms of production simulation. The single trajectory simulation of the complex

(ligand and TPI enzyme) in explicit solvent, was then decomposed by removing appropriate atoms to obtain energy parameters for the free ligand (sulfaE) and TPI enzyme (Eq. (1)) (Ren *et al.*, 2020). The uncertainties for thermodynamic parameters of interest are obtained from statistical analysis using energy data from the 500 sampled conformations. The entropic contributions (Eq. (2)), are not computed because the ligand and proteins are similar and inclusion has limited impact on ranking of relative binding affinities as observed by multiple studies (Wang *et al.*, 2018; Yang *et al.*, 2011).

## RESULTS AND DISCUSSION

In order to elucidate the selectivity and affinity essential to the binding of sulfaE to *Plasmodium* and human TPI glycolytic enzymes, an energetic analysis using a combination of MD simulations and MM/PBSA free energy computation method was used. To calculate the binding free energies, molecular conformations obtained from the MD simulations of the four AutoDock initial complexes were used. After 500 ns of MD simulations, 500 conformations from each equilibrated complex was used to compute the average binding energy and energetic contribution for each amino acid residue in enzyme binding sites using the MM-PBSA method.

### Structural stability of complexes

To monitor the stability of the systems, the total energy ( $E_T$ ) and root means square deviation (RMSD) was investigated (Fig. 4). The average values of  $E_T$  within the first 100 ns and rest of simulations not shown in Fig. 4 are: (hTPI-active site complex;  $-8.36 \times 10^5$  kJ/mol, hTPI-dimer interface complex;  $-5.20 \times 10^5$  kJ/mol, pTPI-active site complex;  $-5.27 \times 10^5$  kJ/mol, pTPI-dimer interface complex;  $-7.72 \times 10^5$  kJ/mol). The six systems (apo forms of the enzymes and four complexes) were also stable during simulation with deviations from average structures ranging from 1.0 to 2.5 Å (Fig. 4). The average backbone RMSD ranges from 1.0 Å (unbound hTPI, pTPI, and hTPI-active site complex), 1.5 Å for the dimer interface complexes, to 2.0 Å for the pTPI dimer interface.

It is evident from Fig. 4 that the presence of SulfaE ligand in the different binding pockets causes slight structural changes. The hTPI complexes fluctuate less compared to the pTPI (Fig. 4).

An estimated measure of flexibility for each residue in all four complexes is shown in Fig. 5 below. This measure of residue flexibility is similar hTPI, pTPI and the four complexes with some regions showing minimal residue fluctuations (within 1.5 Å) while some show significant residue fluctuations (2–4 Å). In general, we observed more significant fluctuations in regions or with residues in close or direct contact with the binding ligand sulfaE. The residues around loop 6 of the TPI enzyme (160–200) are known to be involved with catalysis and showed more fluctuations in the neighborhood of 2.0–3.5 Å with the apo forms of the enzymes. The sulfaE/pTPI active site complex also shows fluctuations between 2.0 and 2.7 Å. The dimer interface residues (40–80) for interaction with pTPI show dynamic fluctuations within 2 Å. It is important to determine whether these overall residue movements contribute to molecular binding or are just

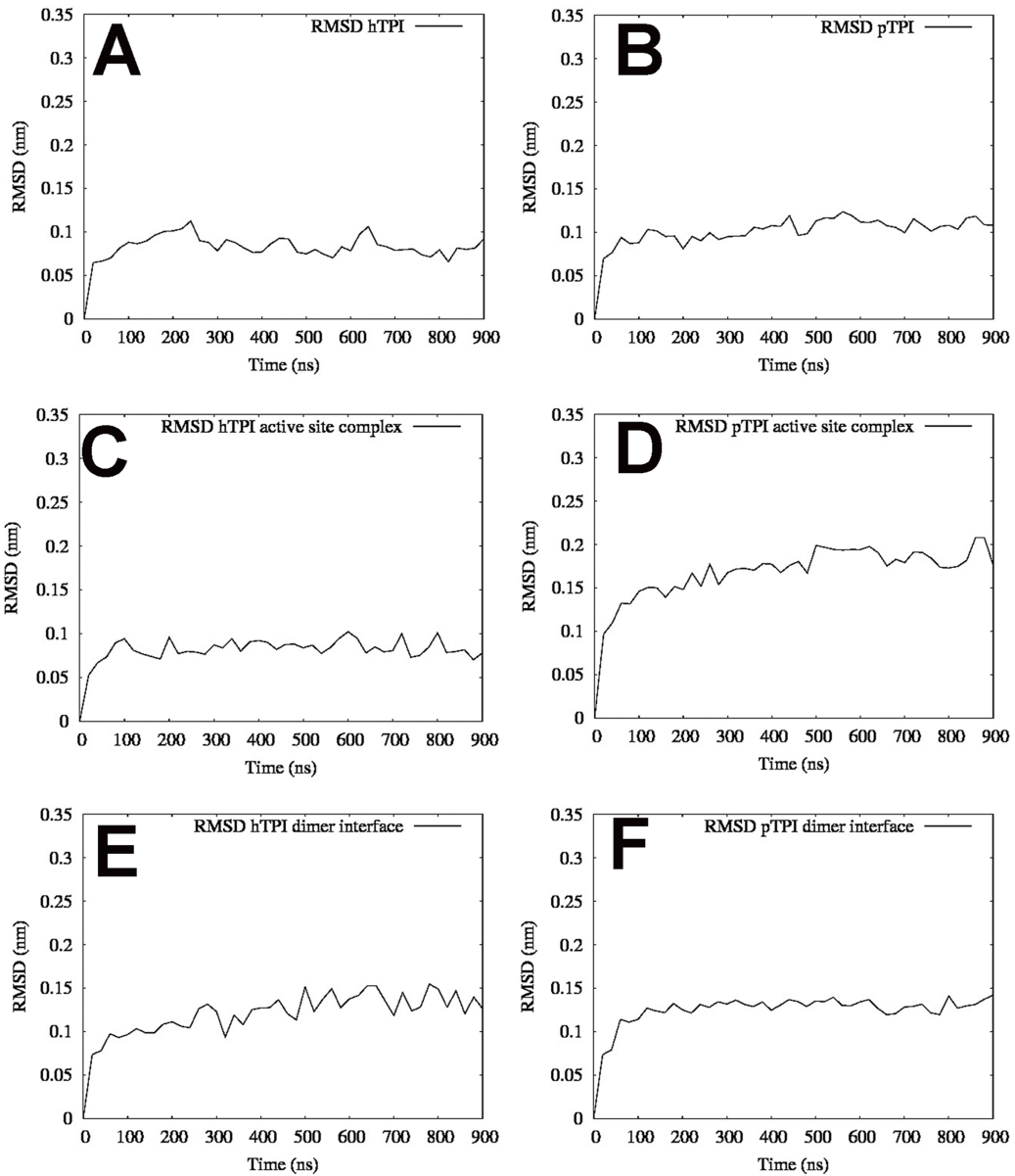


**Figure 4 Root-mean-square deviation.** Time evolution of root-mean-square deviations of backbone atoms relative initial conformation for sulfaE/TPI complexes (A) Free-hTPI (B) Free-pTPI (C) hTPI active site complex (D) pTPI active site complex. (E) hTPI dimer interface complex. (F) pTPI-dimer interface complex.

Full-size DOI: [10.7717/peerj-pchem.13/fig-4](https://doi.org/10.7717/peerj-pchem.13/fig-4)

random molecular motions. This seems to some stabilization of residue fluctuations prevalent within TPI loop 6 residues and dimer interface residues and therefore indicate some impact in the ligand binding process.

### Binding free energy

Five hundred conformations from 500 to 900 ns of the simulations were collected and used for the MM-PBSA calculations. The binding energies of the interaction between the ligands and enzymes are presented in Table 2 and Fig. 6. More negative binding energies,

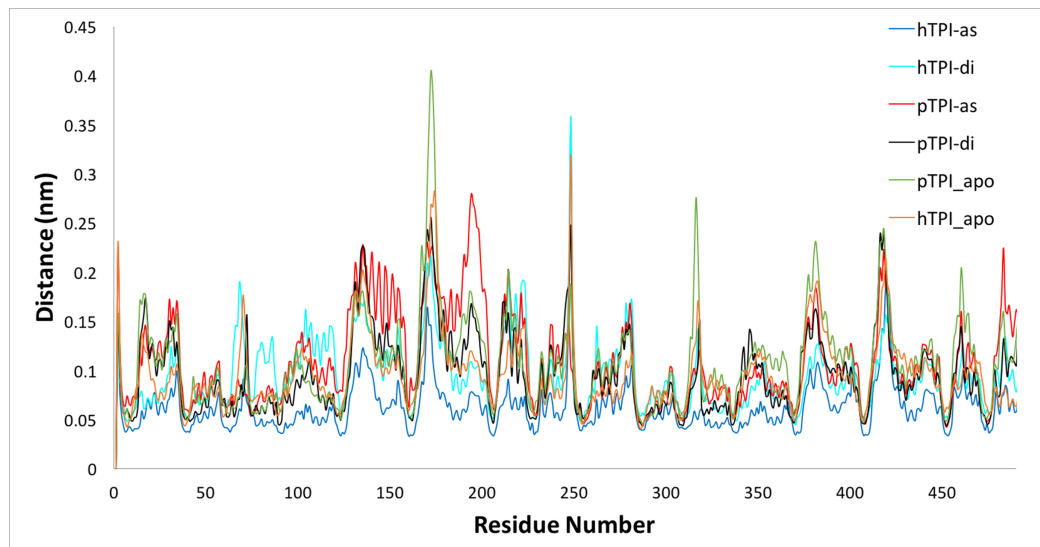


**Figure 5** Root-mean-square fluctuations of hTPI and pTPI complexes with sulfaE. Residues 1–248 correspond to chain A and residues 249–496 chain B. [Full-size](#) DOI: 10.7717/peerj-pchem.13/fig-5

**Table 2** MM-PBSA score for the four complexes formed between SulfaE and hTP/pTPI.

Energy terms	hTPI-energy (kJ/mol)		pTPI-energy (kJ/mol)	
	Active site region	Dimer interface	Active site region	Dimer interface
$\Delta G_{\text{bind}}$	$-116.79 \pm 2.18$	$-41.32 \pm 1.20$	$-71.62 \pm 3.69$	$-42.91 \pm 1.06$
$\Delta E_{\text{elec}}$	$-107.67 \pm 2.18$	$-84.40 \pm 3.96$	$-45.17 \pm 1.74$	$-20.41 \pm 1.81$
$\Delta E_{\text{vdW}}$	$-98.18 \pm 1.79$	$-50.44 \pm 0.86$	$-96.24 \pm 3.53$	$-96.92 \pm 2.04$
$\Delta E_{\text{PolarSol}}$	$100.14 \pm 2.10$	$101.69 \pm 3.09$	$80.08 \pm 2.79$	$86.38 \pm 2.19$
SASA	$-11.18 \pm 0.20$	$-8.19 \pm 0.12$	$-10.00 \pm 0.35$	$-10.98 \pm 0.19$
SAV	$0.00 \pm 0.00$	$0.00 \pm 0.00$	$0.00 \pm 0.00$	$0.00 \pm 0.00$
WCA	$0.00 \pm 0.00$	$0.00 \pm 0.00$	$0.00 \pm 0.00$	$0.00 \pm 0.00$

**Note:**

$\Delta E_{\text{elec}}$ , electrostatic energy;  $\Delta E_{\text{vdW}}$ , Van der Waals energy;  $\Delta E_{\text{PolarSol}}$ , polar solvation energy; SASA, non-polar solvation energy.

correlate with a favorable binding of sulfonamide to the TPI binding pocket. According to the binding energies ( $\Delta G_{\text{bind}}$ ), the complexes at the active site of the TPI enzymes are more favorable than the dimer interface complexes. There is a slight preference for binding to pTPI as opposed to hTPI. The binding energy contributions from electrostatics, Van der Waals and hydrophobic effects are also presented in Table 2. Overall favorable binding is enhanced by energetic contributions from hydrogen bonding, intermolecular electrostatic, Van der Waals interactions and the non-polar component of the free energy of solvation (SASA) including hydrophobic effects (Table 2). The active site (AS) region for both enzyme species show strong affinity with sulfaE (Fig. 6) that is sustained throughout the entire simulation. The electrostatic component of the binding energy is responsible for stronger interactions at the active site of hTPI compared to pTPI. The enhanced binding observed with pTPI compared to hTPI is more pronounced at

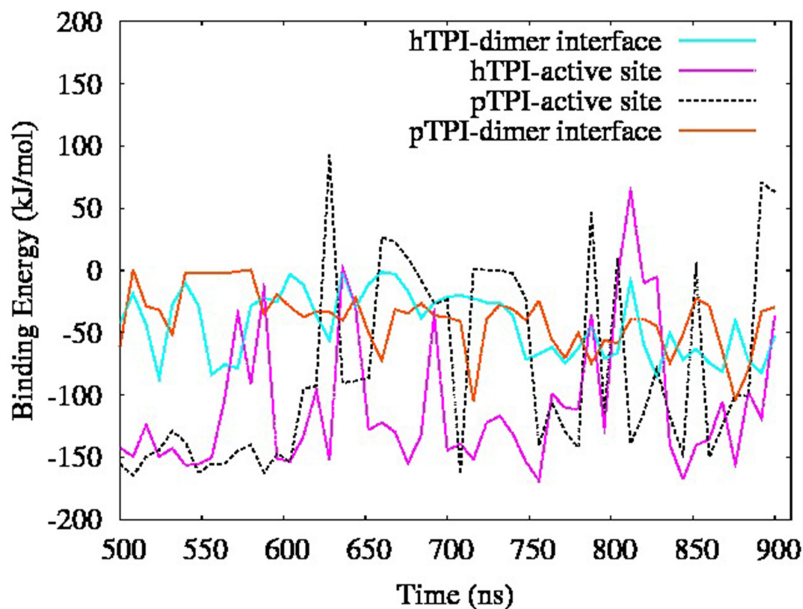


**Figure 6** Binding energy last 400 ns of simulation. The cyan curve represents the binding energy (pTPI-Active Site), pink (hTPI-Active Site), black (pTPI-dimer interface), blue (hTPI-dimer interface).

[Full-size](#) DOI: [10.7717/peerj-pchem.13/fig-6](https://doi.org/10.7717/peerj-pchem.13/fig-6)

the dimer interface. The unfavorable desolvation energy for the polar groups, the van der Waals, polar solvation energies and hydrophobic effects are the reasons we observe difference in binding between hTPI and pTPI.

### Binding modes and residue contributions to binding process

The interactions of sulfaE with the binding sites of hTPI and pTPI are shown in Figs. 7 and 8. The complexes are stabilized in each pocket by a combination of polar and non-polar amino acid residues located within 5 Å directed by hydrogen bonding, electrostatics and Van der Waals interactions. The MD simulations revealed close contact interactions of sulfaE with T216, L226, S211, E212, P178, T175, T177, Y208 at the active site of hTPI. For the dimer interface of hTPI E77, N65, F102, R98 were revealed.

For pTPI complexes, Q64, N65, S45, V44, Y48, V78 and K112 interact with ligand in dimer interface, while L113, K122, L162, I161, V125 and F150 interact at the active site. The mix in polarity of close contact residues as well as the dipolar nature of the sulfonamide ligand structure is in line with the strong contributions of the Van der Waal and electrostatic interactions to the overall binding energy. Multiple hydrogen bonds are formed between sulfaE and TPI enzymes. The hydrogen bond occupancy is however higher in the active site complexes compared to the dimer interface complexes. In addition, the perceived bias in affinity towards pTPI maybe a result dimer interface complex been stabilized by the 98% hydrogen bond occupancy between sulfaE nitrogen atom acceptors and Q64. For the hTPI dimer interface the N65 hydrogen bond only shows a 33.6% occupancy during the simulation (Table 3). The active site complexes for both

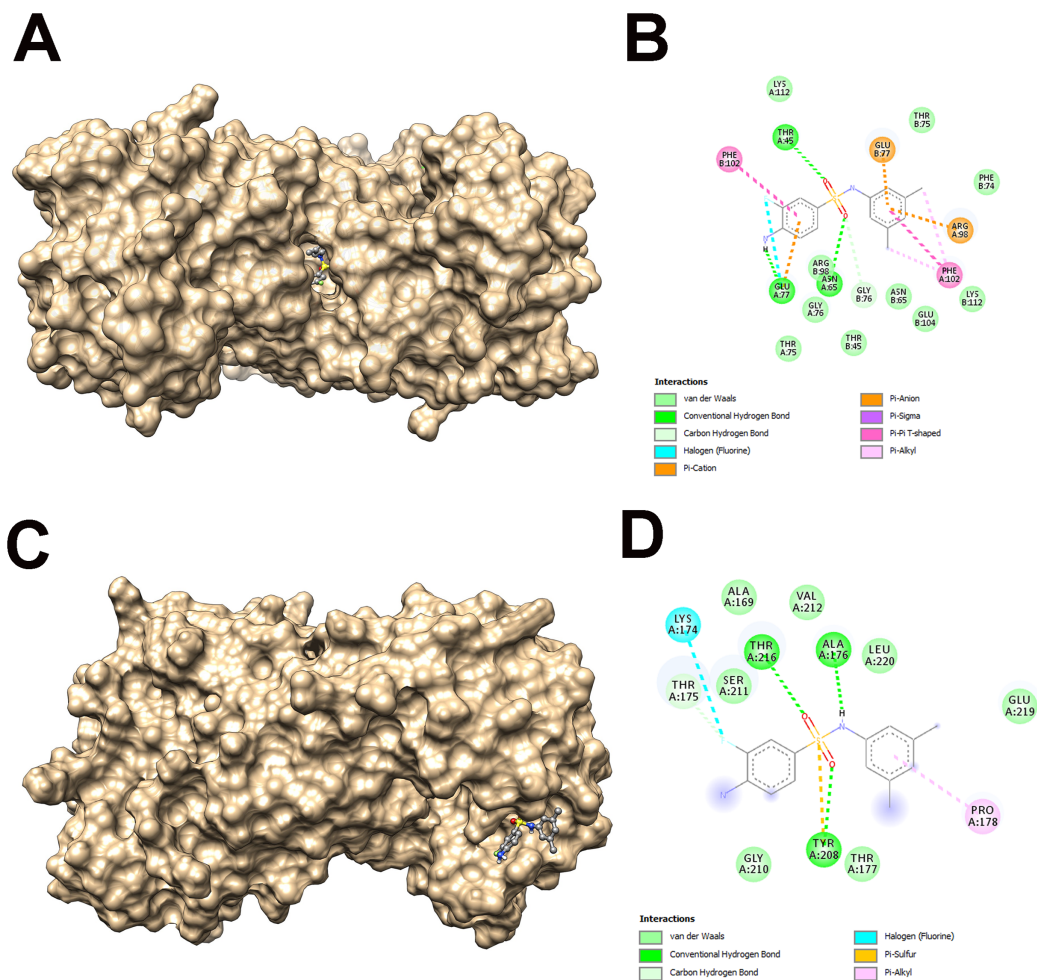


**Figure 7** Complex showing interaction between sulfaE and hTPI. (A) hTPI-dimer interface binding pocket. (B) 2D ligand interaction diagram showing dimer interface residues. (C) hTPI-Active Site. (D) 2D ligand interaction diagram showing active site residues.

Full-size DOI: [10.7717/peerj-pchem.13/fig-7](https://doi.org/10.7717/peerj-pchem.13/fig-7)

enzymes (hTPI and pTPI) form multiple hydrogen bonds averaging above 95% occupancy during the simulations (Table 3).

Per-residue energy decomposition over the same time intervals used to determine the binding energy calculations, was to estimate the impact of residue substitutions between hTPI and pTPI on binding. The decomposed energy contributions from individual TPI residues are presented in the sulfaE-residue interaction map (Figs. 9 and 10). The maps vividly show the cluster of residues in each enzymes pocket and their contribution to binding. For example we observe that the dimer interface residues (46–50, 75–80) in pTPI contribute more to binding compared to hTPI dimer interface residues (Figs. 9 and 10; Table 4). The active site binding residues (95–98, 160–167) also show strong contributions in both species. The maps suggest that the stronger affinity observed with the pTPI dimer interface compared to the hTPI dimer interface is due to some cooperative effect between residues from both monomeric units of TPI.

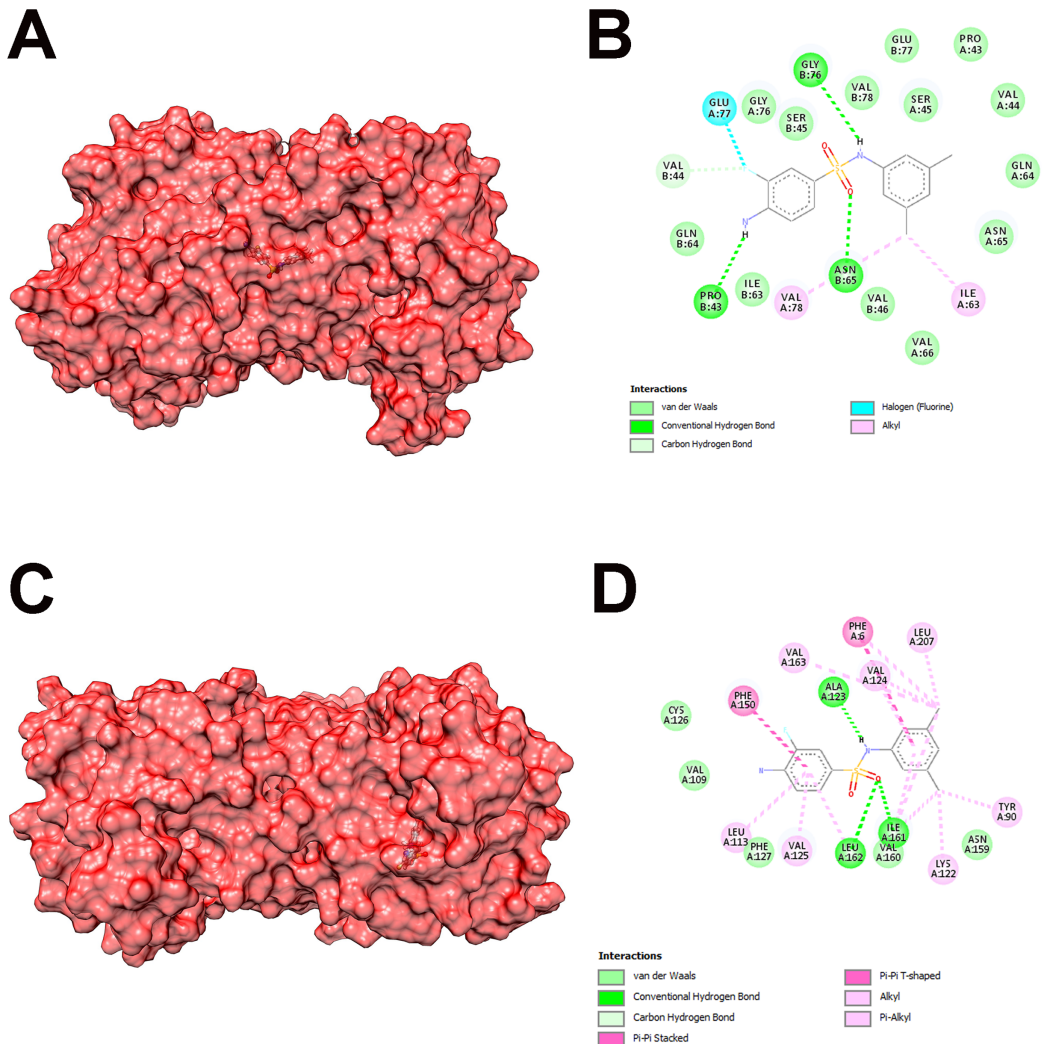


**Figure 8** Complex showing interaction between sulfaE and pTPI. (A) pTPI-dimer interface binding pocket. (B) 2D ligand interaction diagram showing dimer interface residues. (C) pTPI-Active Site. (D) 2D ligand interaction diagram showing active site residues with ligands.

Full-size DOI: 10.7717/peerj-pchem.13/fig-8

## DISCUSSION

The observations from this study also mirror literature findings that the glycolytic enzyme TPI is a potential target for refinement of antimalarial chemotherapies (*Kim & Dang, 2005*). A number of experiments have shown that glycolytic enzyme like TPI can be selectively targeted by antimalarial agents (*Astorga et al., 2012; Gayathri et al., 2009*). In a previous study using blind docking with the AutoDock4.2 software, differences in the interactions between a number of sulfonamides and hTPI/pTPI were observed in the micromolar subrange, suggesting two main binding motifs. The first goal of this work was to obtain an energetic description of the interactions between a novel sulfonamide ligand representative and hTPI or pTPI. Specifically, we questioned the nature of the interactions given those similarities in binding domains between TPI enzymes across

**Table 3** Hydrogen bond occupancy for each residue in their respective complexes.

Hydrogen bond occupancy active site			Hydrogen bond occupancy dimer interface		
Ligand	hTPI	%	Ligand	hTPI	%
249-H2	A-176-O	97.6	249-H2	E-77-OE1	26.7
249-H	K-174-O	38.1	249-H	F-102-O	24.4
249-01	T-216-HG1	95.7	249-O	R-98-H11	33.9
249-0	Y-208-HH	94.2	249-O	N-65-D21	33.6
Ligand	pTPI	%	Ligand	pTPI	%
249-H2	I-161-O	98.4	249-O	G-75-H	20.8
249-H	Q-146-O	37.2	249-O	P-43-O	29.8
249-01	V-125-HN	94.0	249-O	N-65-D21	46.5
			249-N	Q-64-HN	98.6

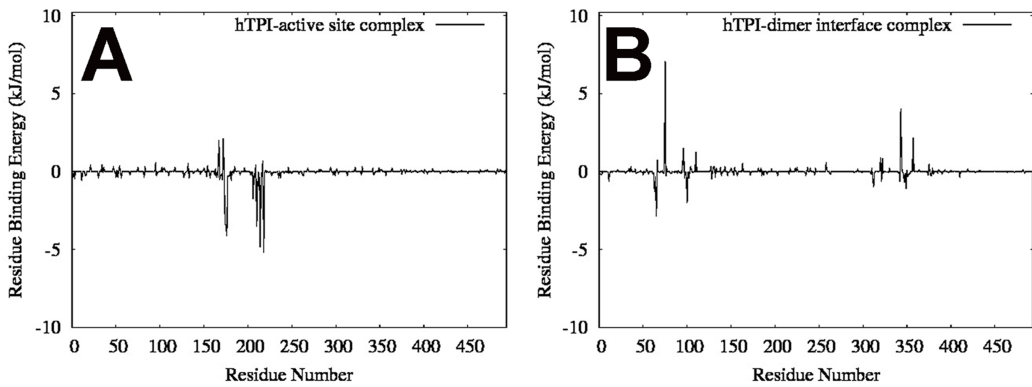


**Figure 9** Individual residue contribution to the binding energy for each complex. Residues 1–248 corresponds to chain A and residues 249–496 correspond to chain B. (A) hTPI-Active Site binding energy contribution from residues, (B) hTPI-dimer interface residue contribution.

Full-size DOI: [10.7717/peerj-pchem.13/fig-9](https://doi.org/10.7717/peerj-pchem.13/fig-9)

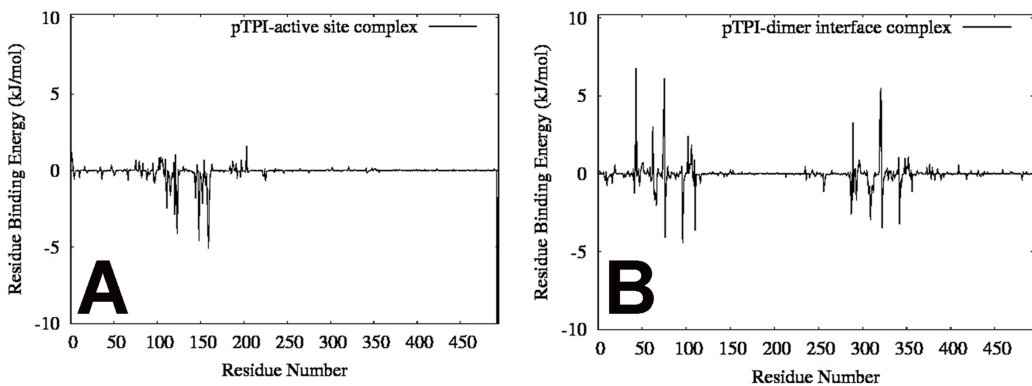


**Figure 10** Individual residue contribution to the binding energy for each complex. Residues 1–248 corresponds to chain A and residues 249–496 correspond to chain B. (A) pTPI-Active Site binding energy contribution from residues, (B) pTPI-dimer interface residue contribution.

Full-size DOI: [10.7717/peerj-pchem.13/fig-10](https://doi.org/10.7717/peerj-pchem.13/fig-10)

**Table 4** Decomposition of Binding Free Energies  $\Delta G$  (kJ/mol) for the four SulfaE–pTPI Complexes into Contributions from Individual Residues.

Residue	MM energy	Polar energy	Apolar energy	Total energy
SulfaE-pTPI dimer interface complex (kJ/mol)				
VAL-A44	-1.36	1.79	-0.047	0.38
VAL-B44	-4.10	2.47	-0.76	-1.70
SER-A45	-7.04	14.50	-0.68	6.79
SER-B45	-8.07	11.94	-0.59	3.29
VAL-A46	-0.78	0.65	-0.0047	-0.129
VAL-B46	-1.70	0.56	-0.065	-1.21
HIS-A47	-0.22	0.17	0.00	-0.054
HIS-B47	-0.069	0.35	0.00	0.28
TYR-A48	-0.21	0.44	0.00	0.24
TYR-B48	-0.12	0.44	0.00	0.31
GLN-A64	-2.99	6.16	-0.16	3.00
GLN-B64	-7.51	6.90	-0.18	-0.79
ASN-A65	-5.84	5.63	-0.52	-0.73
ASN-B65	-13.23	10.92	-0.64	-2.96
VAL-A66	-1.75	0.19	-0.056	-1.61
VAL-B66	-0.37	-0.62	-0.0035	-0.99
SER-67	-1.31	0.015	-0.0003	-1.29
LYS 68	-1.68	-0.38	0.00	-2.05
GLU-A77	1.98	4.24	-0.10	6.11
GLU-B77	-3.42	9.03	-0.097	5.51
VAL-A78	-5.77	2.31	-0.63	-4.09
VAL-B78	-4.43	1.39	-0.44	-3.48
LYS-A112	-2.43	-1.22	0.00	-3.66
LYS-B112	-2.76	1.59	0.00	-1.17
SulfaE-pTPI active site region complex (kJ/mol)				
LEUA-113	-4.54	0.73	-0.45	-0.43
LEUA117	-2.28	0.49	-0.32	-2.11
LYS-A122	-2.93	3.71	-0.45	0.31
ALA-A123	-4.12	8.70	-0.50	4.09
VAL-A124	-6.41	1.31	-0.094	-5.20
VAL-A125	-9.64	5.45	-0.53	-4.71
PHE-A127	-2.49	0.68	-0.18	-1.99
PHE-A150	-9.67	2.07	-0.72	-8.31
ILE-A154	-3.46	0.36	-0.31	-3.42
VAL-A160	-8.21	2.74	-0.35	-5.82
ILE-A161	-13.91	9.42	-0.52	-5.00
LEU-162	-5.33	1.12	-0.23	-4.44

different species: Is there some selective enhancement for the binding of sulfonamide to hTPI as opposed to pTPI? The mechanism of substrate/ligand interaction by TPI has been studied extensively and shows that the 11 residues in loop 6 and catalytic residues (E165, H95, K12, Y208, A176) are responsible for strong affinity to substrate (Derreumaux & Schlick, 1998; Joseph, Petsko & Karplus, 1990; Roland et al., 2015). Gao et al. (1998) showed that sulfonated dyes (suramin, Direct red 23, Direct Violet 51) interfere with the dimerization process to form biological functional units of TPI thus inhibiting the enzymes. The affinities shown by these sulfonated dyes when interacting with active site residues of TPI ranges from  $-17.7$  to  $-38.8$  kcal/mol with  $IC_{50}$  values ranging from  $41.9$  to  $49.7$   $\mu M$  (Joubert, Neitz & Louw, 2001).

In this study, using a representative sulfonamide sulfaE, the simulations revealed that sulfaE binds TPI with binding free energies ranging from  $-80.45$  kJ/mol ( $-19.2$  kcal/mol) to  $-144.59$  kJ/mol ( $-34.4$  kcal/mol) (Fig. 6). The molecular dynamics simulations and free energy calculations using the MM-PBSA method also suggest that there is selective enhancement in interactions between sulfaE and TPI from human and *Plasmodium* species. The observed bias in interactions is mainly because of the difference in electrostatic and van der Waal interactions at the active site and the dimer interface of both enzymes (Tables 2–4). For the dimer interface complexes, the Van der Waals interaction energy, nonpolar solvation energy, is more favorable for sulfaE-pTPI dimer complex than sulfaE-hTPI complex, shifted by  $-46.48$  kJ/mol and  $-2.79$  kJ/mol respectively (Table 2). The polar solvation energy of sulfaE-hTPI complex is shifted by  $15.31$  kJ/mol relative to the sulfaE-pTPI dimer interface complex. This suggest that a bigger penalty is paid for desolvating the ligand in hTPI compared to pTPI. The intermolecular electrostatic interactions are more favorable for the hTPI complexes especially for the active site complexes. The hydrogen bond occupancy map (Table 3) also shows the formation of four hydrogen bonds with active site complexes with over 90% occupancy during the simulation. The probability of forming hydrogen bonds is lowest with the hTPI-dimer interface complex. The unfavorable polar solvation energy and low H-bond occupancy explains the slight preference sulfaE to interact with the parasitic enzyme compared to its human counterpart. This can open doors for fine-tuning and developing selective and potent ligands the other goal of this study.

The second major goal of this study was to understand the structural motifs responsible for the binding, and whether key TPI residue substitutions are critical for binding sulfonamides. The dimer interface of pTPI with polar and hydrophobic amino acid residues (V44, S45, V46, Y48, I63, Q64, N65, V66, E77, V78) of appropriate sizes seems to form an important binding pocket. The dimer interface for hTPI does have some residue substitutions that make binding difficult (P44, T45, A46, I48 and F74, F102). For example, the V44P substitution leads to a less favorable contribution to Van der Waals, and non-polar contributions to the binding energy for this residue in hTPI (Table 4). A drastic reduction in contribution to these intermolecular interactions is also observed for the S45T, V46A substitutions. The contributions from H47Y, Y48I substitutions are not significantly different across the species. In all these substitutions, the polar solvation energy is less favorable for the hTPI complex. The binding energy individual residue map

**Table 5** Decomposition of binding free energies  $\Delta G$  (kJ/mol) for the four SulfaE–hTPI complexes into contributions from individual residues.

Residue	MM energy	Polar energy	Apolar energy	Total energy
SulfaE-hTPI dimer interface complex (kJ/mol)				
PRO-A44	-0.15	-0.66	0.00	-0.80
PRO-B44	0.059	-0.77	0.00	-0.71
THR-A45	-0.14	-1.01	0.00	-1.45
THR-B45	0.055	-1.24	0.00	-1.19
ALA-A46	-0.048	-0.40	0.00	-0.44
ALA-B46	0.0012	-0.53	0.00	-0.53
TYR-A47	-0.065	-0.11	0.00	-0.17
TYR-B47	0.0072	-0.063	0.00	-0.055
ILE-A48	-0.052	-0.46	0.00	-0.51
ILE-B48	-0.0080	-0.34	0.00	-0.34
ASN-A65	-9.33	8.77	-0.48	-1.04
ASN-B65	0.27	-2.02	-0.022	-1.78
TYR-A67	-5.60	0.83	-0.65	-5.42
TYR-B67	-4.41	2.98	-0.72	-2.15
GLU-A77	-14.50	70.38	-0.63	55.25
GLU-B77	-11.64	39.08	-0.68	26.84
ARG-A98	-16.30	29.12	-0.94	11.87
ARG-B98	3.00	-10.37	-0.33	-7.69
PHE-A102	-3.46	0.27	-0.27	-3.46
PHE-B102	-2.48	1.11	-0.34	-1.71
LYS-A112	-5.40	13.24	-0.071	7.77
LYS-B112	2.74	-3.48	-0.075	-0.83
SulfaE-hTPI active site region complex (kJ/mol)				
THR-A175	-6.59	7.44	-0.96	-0.11
ALA-A176	-13.52	10.57	-0.47	-3.42
THR-A177	-5.96	2.82	-0.27	-3.41
PRO-A178	-5.51	1.88	-0.50	-4.13
TYR-A208	-8.47	6.89	-0.17	-1.75
SER-A211	-7.72	8.94	-0.80	0.43
VAL-A212	-4.62	1.12	-0.0069	-3.51
THR-A216	-11.82	7.97	-0.99	-4.84
LEU-A220	-6.06	1.04	-0.18	-5.20

also shows that more residues contribute favorably to the binding in pTPI compared to hTPI in the active site binding pocket (Figs. 9 and 10). For active site region complexes, only chain A residues where the ligand was docked show active contribution to binding. For the dimer interface pocket, we observe residue contributions from both chains. This indicates that the ligand is forming multiple contacts with key residues on both chains A and B. The dimer interface residues for pTPI, however, contribute more favorably to

the binding energy compared to hTPI residues. For example, the switch in residue from S45T in pTPI to hTPI has a significant effect in contributions from intermolecular electrostatic forces, Van der Waal forces, non-polar and polar desolvation energies.

Specifically, S45 in pTPI contributes favorably to binding with favorable electrostatic and van der Waals energies (-7.04 chain A and -8.04 chain B) compared to T45 with contributions (-0.14 chain A and 0.055 chain B) (Tables 4 and 5). This suggest the larger size of T45 in hTPI is negatively impacting the binding. The affinity of hTPI dimer interface residues is likely dampened by steric factors of the pocket as shown with strong polar solvation energies for some residues like E77. The contribution from each residue indicates that strong and favorable electrostatics and van der Waals interaction overcome the polar solvation energies for interaction between sulfaE and pTPI more readily, explaining the favorable strong total binding energies relative to those between sulfaE and hTPI. Structures of the proposed binding conformations also explain why pTPI seemingly interacts more with sulfaE (Figs. 7 and 8). The ligand sulfaE seems more tightly packed and fits well in the dimer interface of pTPI permitting stronger electrostatic and Van der Waals interactions with the protein residues. The strength of interactions is also bolstered by the contributions from residues in both chains A and B of pTPI. The sulfaE ligand does not benefit from strong contributions from residues in both chains in the hTPI interface (Tables 4 and 5; Figs. 9 and 10). There is a slight shift in the ligand position in hTPI compared to pTPI Figure (Figs. 7 and 8). The ligand sulfaE is also not tightly packed in the dimer interface due to size of hTPI and poor fit because of unfavorable interactions with anchor residues (E77). The fact that mostly residues on one of the monomers contribute significantly towards overall binding energy is also an indicative of fewer favorable interactions with hTPI (Fig. 7; Table 5). We observed that Van der Waals and electrostatic interactions are key components explaining the stronger affinity towards pTPI as opposed to hTPI. In addition, the overall charge of pTPI of (-8e) as opposed to (-6e) for hTPI indicates that subtle residue substitutions do have an observable effect on charge variation between hTPI and pTPI. This charge difference in protein receptor and the dipolar nature of the amine-based sulfaE can lead to selectivity in sulfaE hTPI/pTPI complexes.

## CONCLUSIONS

In this article, we have studied the binding of sulfaE and TPI from human and *Plasmodium* species with complexes formed at two binding pockets; dimer interface and active site region. The total binding energy of interactions was obtained from 900 ns MD simulations in explicit water. This was followed by implicit solvent free energy calculations using the MM-PBSA method. Many experiments have shown that TPI is a potential glycolytic enzyme for the development of antimalarial medication. The similarity in structural folds of TPI enzyme from human and *Plasmodium* species has, however, slowed down the progress in this field. The models of interaction between a representative sulfonamide and TPI enzyme from *Plasmodium* and human species suggested in this article show that subtle substitutions of residues even with similar polarity and just minimal size effect can lead to variations in contributions to the total binding energy from van der Waal and

electrostatic forces. Strong and favorable intermolecular electrostatic, Van der Waals interactions and increases in non-polar solvation energies are responsible for the selectivity of pTPI with sulfaE compared to hTPI at the dimer interface. The importance of polar solvation energies on a per residue basis shows why structural inspection from our previous docking studies is not enough to characterize such interactions. The huge increase in polar solvation energies, especially for some hTPI dimer interface residues (E77), is also responsible for discriminating between complexes formed. We think this molecule can serve as a pharmacophore for the design of new inhibitors using the identified and subtle differences at the dimer interface and differences in interactions around loop 6 and active site residues.

## INSTITUTIONAL ABBREVIATIONS

<b>MD</b>	Molecular Dynamics
<b>MM-PBSA</b>	Molecular Mechanics Poisson–Boltzmann Surface Area
<b>TPI</b>	Triose Phosphate Isomerase
<b>hTPI</b>	Human Triose Phosphate Isomerase
<b>pTPI</b>	<i>Plasmodium</i> triose phosphate isomerase
<b>SASA</b>	Solvent Accessible Surface Area Approximation
<b>sulfaE</b>	4-amino- <i>N</i> -(3,5-dimethylphenyl)-3-fluorbenzenesulfonamide
<b>RMSD</b>	Root Mean-Squared Deviation

## ADDITIONAL INFORMATION AND DECLARATIONS

### Funding

The authors received no funding for this work.

### Competing Interests

The authors declare that they have no competing interests.

### Author Contributions

- Neville Y. Forlemu conceived and designed the experiments, performed the experiments, analyzed the data, performed the computation work, prepared figures and/or tables, authored or reviewed drafts of the paper, and approved the final draft.
- Joseph Sloop conceived and designed the experiments, analyzed the data, authored or reviewed drafts of the paper, designed and synthesized the sulfonamide ligands, and approved the final draft.

### Data Availability

The following information was supplied regarding data availability:

The raw data including gromacs output files (.xvg file formats) and MM-PBSA energy files (.xvg, .dat) used to characterize the interactions between sulfonamides and the complexes are available in the [Supplemental Files](#). These files are zipped and can easily be

accessed with any Linux machine. The raw data indicates that the dimer interface binding site shows differential binding between Plasmodium and human TPI.

## Supplemental Information

Supplemental information for this article can be found online at <http://dx.doi.org/10.7717/peerj-pchem.13#supplemental-information>.

## REFERENCES

- Astorga B, Ekins S, Morales M, Wright SH. 2012. Molecular determinants of ligand selectivity for the human multidrug and toxin extruder proteins MATE1 and MATE2-K. *Journal of Pharmacology and Experimental Therapeutics* 341(3):743–755 DOI 10.1124/jpet.112.191577.
- Berendsen HJC, Postma JPM, Van Gunsteren WF, DiNola A, Haak JR. 1984. Molecular dynamics with coupling to an external bath. *Journal of Chemical Physics* 81(8):3684–3690 DOI 10.1063/1.448118.
- Bray PG, Barrett MP, Ward SA, De Koning HP. 2003. Pentamidine uptake and resistance in pathogenic protozoa: past, present and future. *Trends in Parasitology* 19(5):232–239 DOI 10.1016/S1471-4922(03)00069-2.
- Briolant S, Almeras L, Belghazi M, Boucomont-Chapeaublanc E, Wurtz N, Fontaine A, Granjeaud S, Fusaï T, Rogier C, Pradines B. 2010. *Plasmodium falciparum* proteome changes in response to doxycycline treatment. *Malaria Journal* 9(1):141 DOI 10.1186/1475-2875-9-141.
- Bussi G, Donadio D, Parrinello M. 2007. Canonical sampling through velocity rescaling. *Journal of Chemical Physics* 126(1):014101 DOI 10.1063/1.2408420.
- Dennington R, Keith T, Millam J. 2009. GaussView. Version 5. Available at [http://www.gaussian.com/g\\_tech/gv5ref/gv5citation.htm](http://www.gaussian.com/g_tech/gv5ref/gv5citation.htm).
- Derreumaux P, Schlick T. 1998. The loop opening/closing motion of the enzyme triosephosphate isomerase. *Biophysical Journal* 74(1):72–81 DOI 10.1016/S0006-3495(98)77768-9.
- Dizala-Mukinay C, Babalola R, Sloop J, Forlemu NY. 2017. Targeting the *Plasmodium falciparum* folate pathway: molecular modeling of the affinity of sulfonamide derivatives and isoforms of dihydrofolate reductase thymidylate synthase. *Journal of Chemical Research* 16(2):68–71.
- Djaman J, Abouanou S, Basco L, Kone M. 2004. Limits of the efficacy of chloroquine and sulfadoxine-pyrimethamine in Northern Abidjan (Côte d'Ivoire): combined in vivo and in vitro studies. *Sante* 14(4):205–209.
- Foloppe N, MacKerell J, Alexander D. 2000. All-atom empirical force field for nucleic acids: I. parameter optimization based on small molecule and condensed phase macromolecular target data. *Journal of Computational Chemistry* 21(2):86–104 DOI 10.1002/(SICI)1096-987X(20000130)21:2<86::AID-JCC2>3.0.CO;2-G.
- Forlemu NY, Watkins P, Sloop J. 2017. Molecular docking of selective binding affinity of sulfonamide derivatives as potential anti-malarial agents targeting the glycolytic enzymes: GAPDH, aldolase and TPI. *Open Journal of Biophysics* 7(1):41–57 DOI 10.4236/ojbphy.2017.71004.
- Frisch MJ, Trucks GW, Schlegel HB, Scuseria GE, Robb MA, Cheeseman JR, Scalmani G, Barone V, Petersson GA, Nakatsuji H, Li X, Caricato M, Marenich A, Bloino J, Janesko BG, Gomperts R, Mennucci B, Hratchian HP, Ortiz JV, Izmaylov AF, Sonnenberg JL, Williams-Young D, Ding F, Lipparini F, Egidi F, Goings J, Peng B, Petrone A, Henderson T, Ranasinghe D, Zakrzewski VG, Gao J, Rega N, Zheng G, Liang W, Hada M, Ehara M,

Toyota K, Fukuda R, Hasegawa J, Ishida M, Nakajima T, Honda Y, Kitao O, Nakai H, Vreven T, Throssell K, Montgomery JA Jr, Peralta JE, Ogliaro F, Bearpark M, Heyd JJ, Brothers E, Kudin KN, Staroverov VN, Keith T, Kobayashi R, Normand J, Raghavachari K, Rendell A, Burant JC, Iyengar SS, Tomasi J, Cossi M, Millam JM, Klene M, Adamo C, Cammi R, Ochterski JW, Martin RL, Morokuma K, Farkas O, Foresman JB, Fox DJ. 2016. *Gaussian 09, Revision A.02.* Wallingford: Gaussian, Inc.

Gao XG, Garza-Ramos G, Saavedra-Lira E, Cabrera N, De Gomez-Puyou MT, Perez-Montfort R, Gomez-Puyou A. 1998. Reactivation of triosephosphate isomerase from three trypanosomatids and human: effect of suramin. *Biochemical Journal* 332(Pt. 1):91–96 DOI 10.1042/bj3320091.

Gayathri P, Banerjee M, Vijayalakshmi A, Balaram H, Balaram P, Murthy MR. 2009. Biochemical and structural characterization of residue 96 mutants of *Plasmodium falciparum* triosephosphate isomerase: active-site loop conformation, hydration and identification of a dimer-interface ligand-binding site. *Acta Crystallographica Section D Biological Crystallography* 65(Pt. 8):847–857 DOI 10.1107/S0907444909018666.

Guerra CA, Snow RW, Hay SI. 2006. Defining the global spatial limits of malaria transmission in 2005. In: Hay SI, Graham A, Rogers DJ, eds. *Advances in Parasitology*. Vol. 62. Waltham: Academic Press, 157–179.

Heinberg A, Kirkman L. 2015. The molecular basis of antifolate resistance in *Plasmodium falciparum*: looking beyond point mutations. *Annals of the New York Academy of Sciences* 1342(1):10–18 DOI 10.1111/nyas.12662.

Homeyer N, Gohlke H. 2012. Free energy calculations by the molecular mechanics poisson–boltzmann surface area method. *Molecular Informatics* 31(2):114–122 DOI 10.1002/minf.201100135.

Hyde JE. 2007. Drug-resistant malaria—an insight. *FEBS Journal* 274(18):4688–4698 DOI 10.1111/j.1742-4658.2007.05999.x.

Jorgensen WL, Chandrasekhar J, Madura JD, Impey RW, Klein ML. 1983. Comparison of simple potential functions for simulating liquid water. *Journal of Chemical Physics* 79(2):926–935 DOI 10.1063/1.445869.

Joseph D, Petsko GA, Karplus M. 1990. Anatomy of a conformational change: hinged “lid” motion of the triosephosphate isomerase loop. *Science* 249(4975):1425–1428 DOI 10.1126/science.2402636.

Joubert F, Neitz AW, Louw AI. 2001. Structure-based inhibitor screening: a family of sulfonated dye inhibitors for malaria parasite triosephosphate isomerase. *Proteins: Structure Function and Bioinformatics* 45(2):136–143 DOI 10.1002/prot.1113.

Kehr S, Sturm N, Rahlf S, Przyborski JM, Becker K. 2010. Compartmentation of redox metabolism in malaria parasites. *PLOS Pathogens* 6(12):e1001242 DOI 10.1371/journal.ppat.1001242.

Kim J-w, Dang CV. 2005. Multifaceted roles of glycolytic enzymes. *Trends in Biochemical Sciences* 30(3):142–150 DOI 10.1016/j.tibs.2005.01.005.

Kollman PA, Massova I, Reyes C, Kuhn B, Huo S, Chong L, Lee M, Lee T, Duan Y, Wang W, Donini O, Cieplak P, Srinivasan J, Case DA, Cheatham TE. 2000. Calculating structures and free energies of complex molecules: combining molecular mechanics and continuum models. *Accounts of Chemical Research* 33(12):889–897.

Matondo SI, Temba GS, Kavishe AA, Kauki JS, Kalinga A, van Zwetselaar M, Reyburn H, Kavishe RA. 2014. High levels of sulphadoxine-pyrimethamine resistance Pfdhfr–Pfdhps

quintuple mutations: a cross sectional survey of six regions in Tanzania. *Malaria Journal* 13(1):152 DOI 10.1186/1475-2875-13-152.

- Menard D, Dondorp A.** 2017. Antimalarial drug resistance: a threat to malaria elimination. *Cold Spring Harbor Perspectives in Medicine* 7(7):a025619 DOI 10.1101/cshperspect.a025619.
- Mulenga M, Malunga F, Bennett S, Thuma PE, Shulman C, Fielding K, Allouche A, Greenwood BM.** 2006. A randomised, double-blind, placebo-controlled trial of atovaquone-proguanil vs. sulphadoxine-pyrimethamine in the treatment of malarial anaemia in Zambian children. *Tropical Medicine and International Health* 11(11):1643–1652 DOI 10.1111/j.1365-3156.2006.01726.x.
- Parthasarathy S, Ravindra G, Balaram H, Balaram P, Murthy MR.** 2002. Structure of the *Plasmodium falciparum* triosephosphate isomerase-phosphoglycolate complex in two crystal forms: characterization of catalytic loop open and closed conformations in the ligand-bound state. *Biochemistry* 41(44):13178–13188 DOI 10.1021/bi025783a.
- Petersen I, Eastman R, Lanzer M.** 2011. Drug-resistant malaria: molecular mechanisms and implications for public health. *FEBS Letters* 585(11):1551–1562 DOI 10.1016/j.febslet.2011.04.042.
- Plowe CV, Roper C, Barnwell JW, Hippi CT, Joshi HH, Mbacham W, Rosenthal PJ.** 2007. World antimalarial resistance network (WARN) III: molecular markers for drug resistant malaria. *Malaria Journal* 6(1):121 DOI 10.1186/1475-2875-6-121.
- Ren J, Yuan X, Li J, Lin S, Yang B, Chen C, Zhao J, Zheng W, Liao H, Yang Z, Qu Z.** 2020. Assessing the performance of the g\_mmpbsa tools to simulate the inhibition of oseltamivir to influenza virus neuraminidase by molecular mechanics poisson–boltzmann surface area methods. *Journal of the Chinese Chemical Society* 67(1):46–53 DOI 10.1002/jccs.201900148.
- Richard JP.** 1985. Reaction of triosephosphate isomerase with L-glyceraldehyde 3-phosphate and triose 1,2-enediol 3-phosphate. *Biochemistry* 24(4):949–953 DOI 10.1021/bi00325a021.
- Ringwald P, Sukwa T, Basco LK, Bloland P, Mendis K.** 2002. Monitoring of drug-resistant malaria in Africa. *Lancet* 360(9336):875–876 DOI 10.1016/S0140-6736(02)09979-8.
- Roland BP, Amrich CG, Kammerer CJ, Stuchul KA, Larsen SB, Rode S, Palladino MJ.** 2015. Triosephosphate isomerase I170V alters catalytic site, enhances stability and induces pathology in a *Drosophila* model of TPI deficiency. *Biochimica et Biophysica Acta (BBA)—Molecular Basis of Disease* 1852(1):61–69 DOI 10.1016/j.bbadiis.2014.10.010.
- Triglia T, Menting JG, Wilson C, Cowman AF.** 1997. Mutations in dihydropteroate synthase are responsible for sulfone and sulfonamide resistance in *Plasmodium falciparum*. *Proceedings of the National Academy of Sciences of the United States of America* 94(25):13944–13949 DOI 10.1073/pnas.94.25.13944.
- Van Der Spoel D, Lindahl E, Hess B, Groenhof G, Mark AE, Berendsen HJ.** 2005. GROMACS: fast, flexible, and free. *Journal of Computational Chemistry* 26(16):1701–1718 DOI 10.1002/jcc.20291.
- Van Gunsteren WF, Berendsen HJC.** 1977. Algorithms for macromolecular dynamics and constraint dynamics. *Molecular Physics* 34(5):1311–1327 DOI 10.1080/0026897700102571.
- Velanker SS, Ray SS, Gokhale RS, Suma S, Balaram H, Balaram P, Murthy MRN.** 1997. Triosephosphate isomerase from *Plasmodium falciparum*: the crystal structure provides insights into antimalarial drug design. *Structure* 5(6):751–761 DOI 10.1016/S0969-2126(97)00230-X.
- Verlinde CLMJ, Hannaert V, Blonski C, Willson M, Périé JJ, Fothergill-Gilmore LA, Opperdoes FR, Gelb MH, Hol WGJ, Michels PAM.** 2001. Glycolysis as a target for the design

of new anti-trypanosome drugs. *Drug Resistance Updates* 4(1):50–65  
DOI 10.1054/drup.2000.0177.

**Wang C, Greene DA, Xiao L, Qi R, Luo R. 2018.** Recent developments and applications of the MMPBSA method. *Frontiers in Molecular Biosciences* 4:87  
DOI 10.3389/fmemb.2017.00087.

**Yang T, Wu JC, Yan C, Wang Y, Luo R, Gonzales MB, Dalby KN, Ren P. 2011.** Virtual screening using molecular simulations. *Proteins: Structure Function and Bioinformatics* 79(6):1940–1951  
DOI 10.1002/prot.23018.

**Zoete V, Cuendet MA, Grosdidier A, Michelin O. 2011.** SwissParam: a fast force field generation tool for small organic molecules. *Journal of Computational Chemistry* 32(11):2359–2368  
DOI 10.1002/jcc.21816.